ADVANCED MATERIALS

Supporting Information

for *Adv. Mater.*, DOI: 10.1002/adma.202006147

Operando Tailoring of Defects and Strains in Corrugated #-$Ni(OH)_2$ Nanosheets for Stable and High-Rate Energy Storage

Shaofeng Li, Nikhil Sharma, Chang Yu, Yan Zhang, Gang Wan, Rong Fu, Hongling Huang, Xueyan Sun, Sang-Jun Lee, Jun-Sik Lee, Dennis Nordlund, Piero Pianetta, Kejie Zhao,* Yijin Liu,* and Jieshan Qiu**

Supporting Information

Operando **tailoring of defects and strains in corrugated β-Ni(OH)$_2$ nanosheets for stable and high-rate energy storage**

Shaofeng Li, Nikhil Sharma, Chang Yu[*]*, Yan Zhang, Gang Wan, Rong Fu, Hongling Huang, Xueyan Sun, Sang-Jun Lee, Jun-Sik Lee, Dennis Nordlund, Piero Pianetta, Kejie Zhao*[*]*, Yijin Liu*[*]*, and Jieshan Qiu*[*]

Experimental Section

Synthesis of NiV-LDH: Firstly, $NiCl_2$ (0.9 mmol), VCl_3 (0.3 mmol), NH_4F (3.3 mmol) and urea (8.3 mmol) were dissolved in 20 mL of deionized water (DI). Then, the solution was poured into a PFTE-lined stainless steel autoclave and maintained at 120 ^oC for 16 h together with the superhydrophilic CFP, which follows our previous work. After the autoclave was naturally cooling down, the CFP was washed with DI and dried in air, yielding the NiV-LDH.

Material characterizations: SEM were measured on FEI NOVA NanoSEM 450. TEM were conducted on FEI Tecnai G2 F30. A Rigaku D/Max 2400 diffractometer with Cu Kα radiation (λ = 1.5406 Å) was used for collecting Powder XRD patterns. XPS analysis was performed on Thermo ESCALAB 250 instrument with an Mg Kα source ($h\nu$ = 1253.6 eV). EQCM were recorded at room temperature (~25 ^oC) with Quartz Crystal Microbalance (QCM25, Princeton Applied Research) and a IVIUM Compactstat in a three-electrode system with the Au quartz resonator working electrode.

Electrochemical characterization: All the electrochemical measurements were evaluated on a standard electrochemical workstation (Bio-Logic SP-200). All the as-made samples were served as working electrode directly, with a Hg/HgO electrode as the reference electrode and a Pt foil as the counter electrode, respectively. The specific capacity of single electrode was calculated based on the GCD curves using following equation:

$$C_s = (\int Idt)/m \quad (1)$$

where C_s (C g^{-1}) is specific capacity, I (A) represents the discharge current, m (g) corresponds to the mass of the active material (the mass of the CFP substrate is not included).

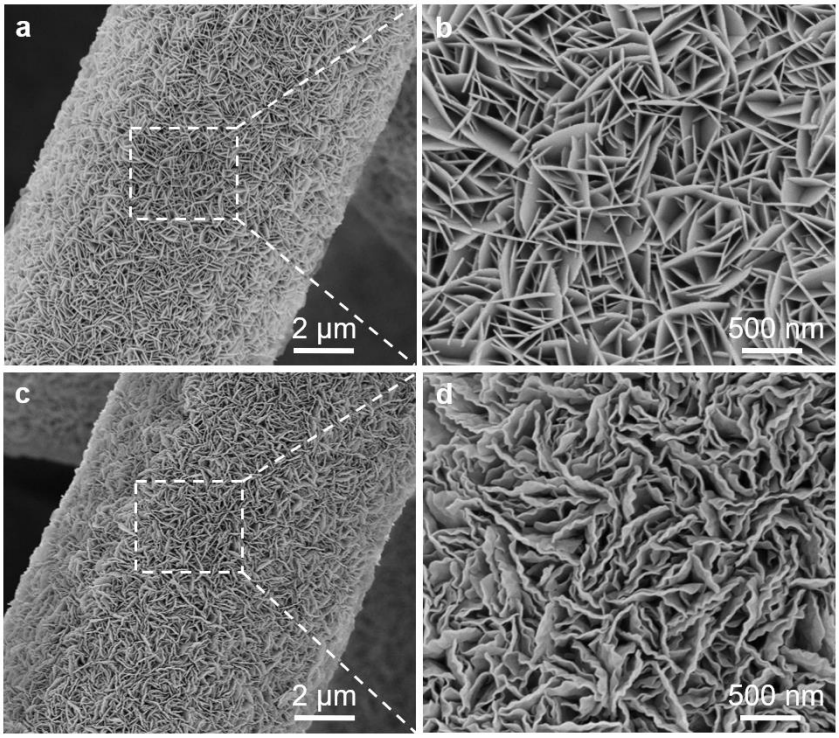

Figure S1. SEM images of a, b) the NiV-LDH and c, d) NiV-LDH after 9th cycle over a voltage window of 0-0.7 V.

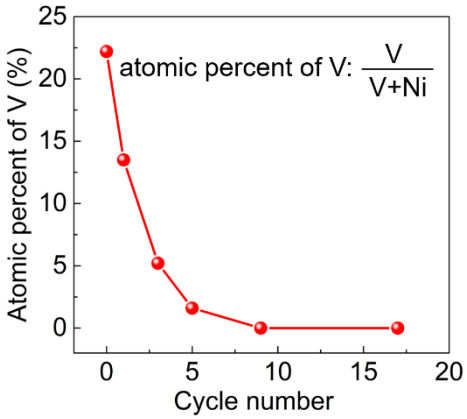

Figure S2. Atomic percent of vanadium in NiV-LDH electrode after different CV cycles within 0-0.7 V.

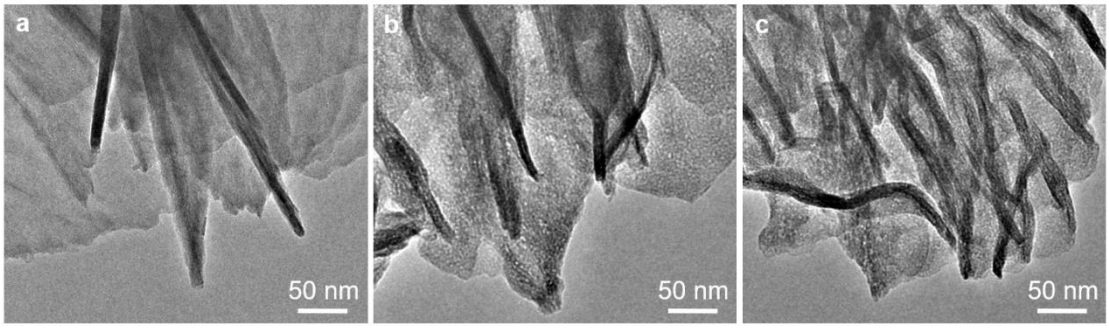

Figure S3. TEM images of a) NiV-LDH electrode, b) 0.7-5 and c) 0.7-9 electrodes.

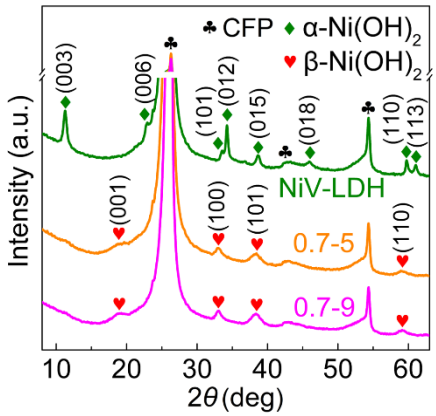

Figure S4. XRD patterns of NiV-LDH, 0.7-5 and 0.7-9.

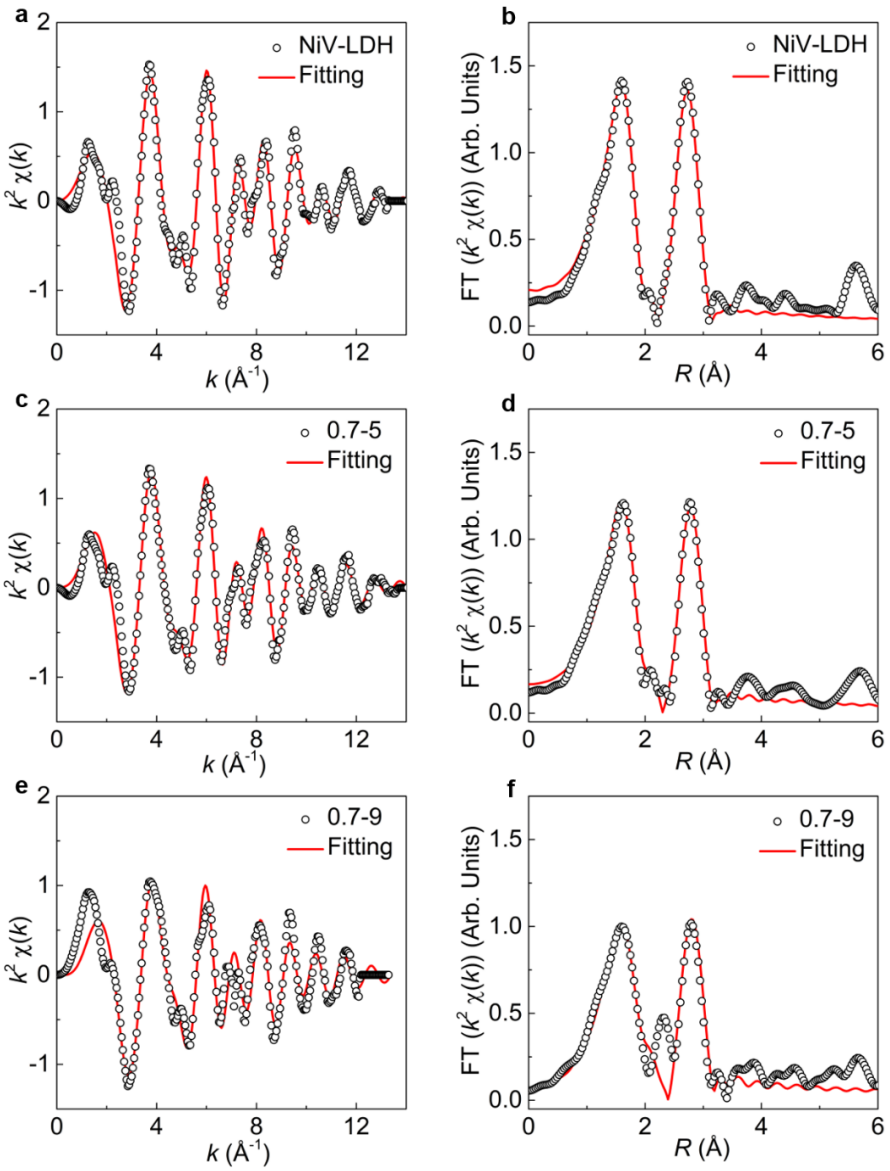

Figure S5. EXAFS $k^2\chi(k)$ oscillation curves and R space fitting results of Ni K-edge for a, b) NiV-LDH electrode, c, d) 0.7-5 and e, f) 0.7-9 electrodes.

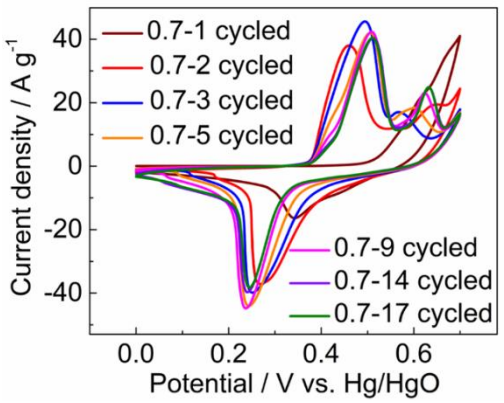

Figure S6. *Operando* CV curves of the NiV-LDH electrode within 0-0.7 V at the scan rate of 5 mV s^{-1}.

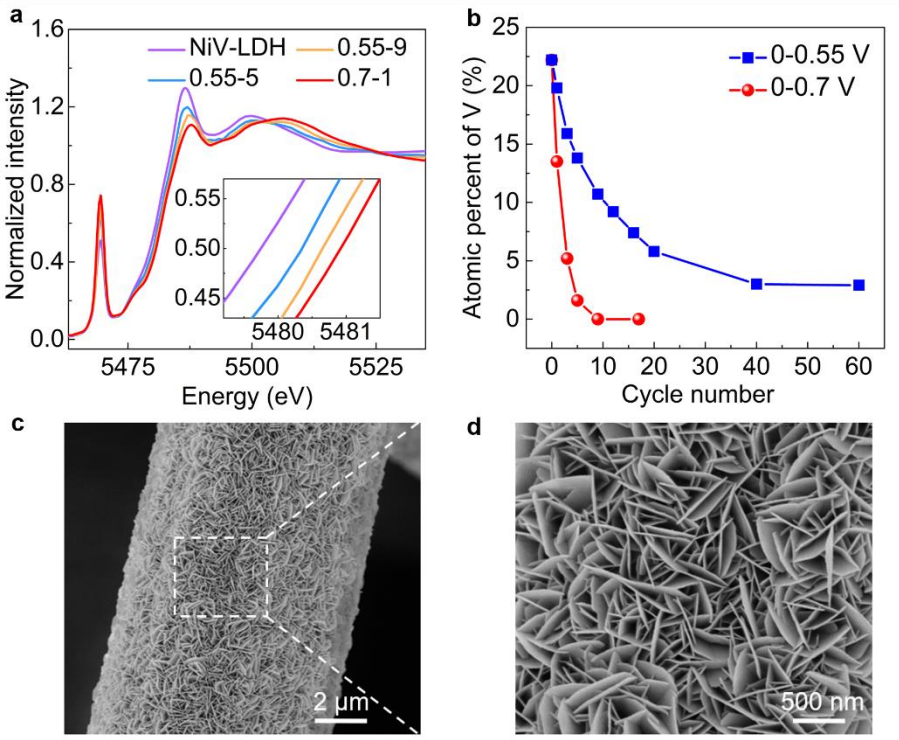

Figure S7. a) *Operando* XANES spectra recorded at the V K-edge after different CV cycles within 0-0.55 V for the NiV-LDH electrode. b) Atomic percent of vanadium in NiV-LDH electrode after different CV cycles within 0-0.55 V and 0-0.7 V. c, d) SEM images of NiV-LDH electrode after 9th cycle over a voltage window of 0-0.55 V.

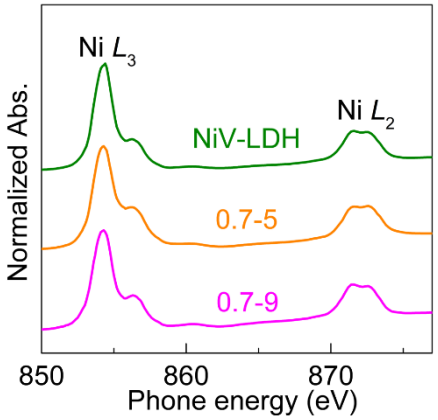

Figure S8. Ni *L*-edge spectra of NiV-LDH under different stages.

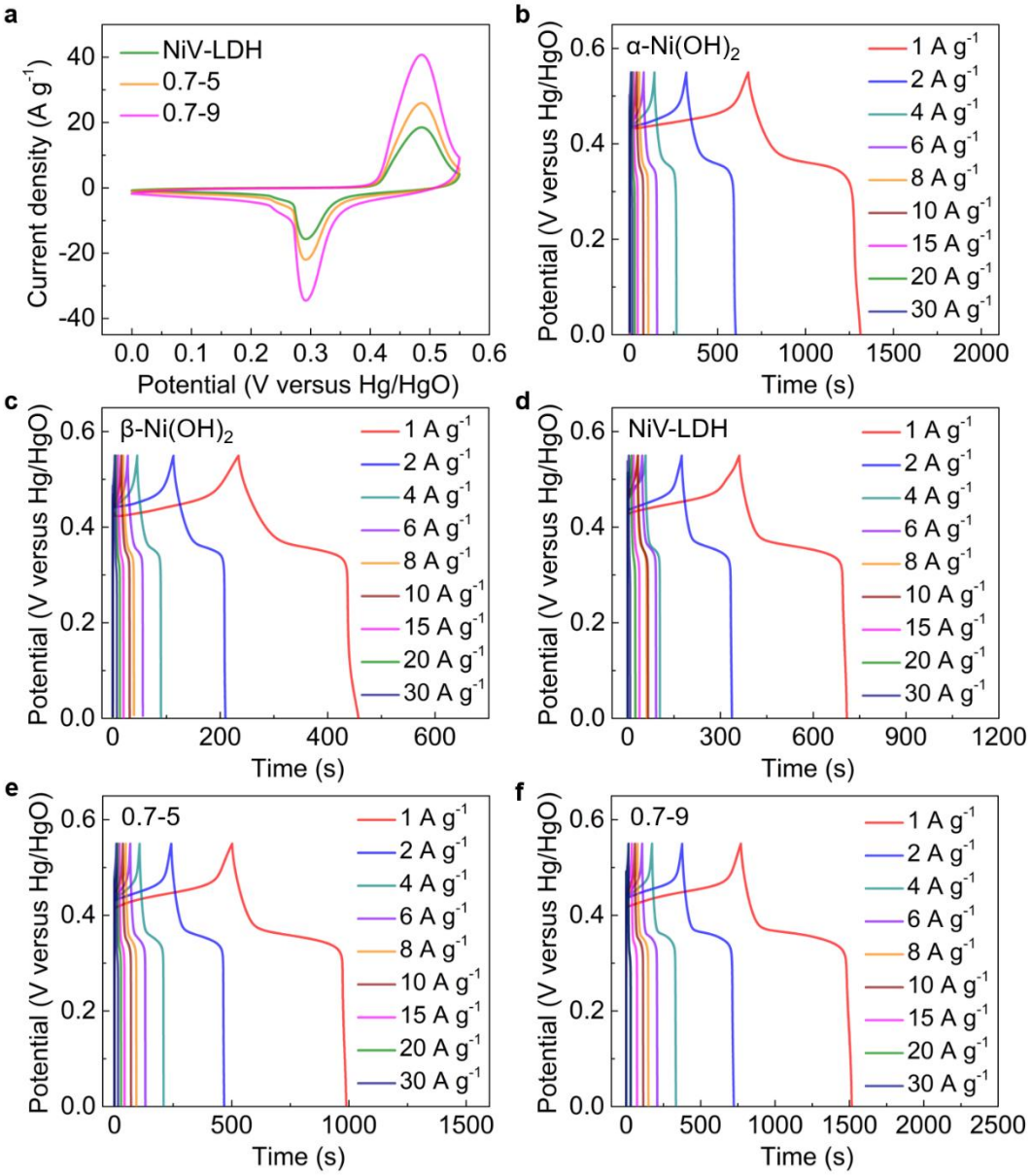

Figure S9. a) CV curves of the NiV-LDH under different stages within 0-0.55 V at the scan rate of 5 mV s^{-1}. GCD curves of b) regular α-$Ni(OH)_2$, c) regular β-$Ni(OH)_2$, d) NiV-LDH, NiV-LDH after e) 5^{th} cycling and f) 9^{th} cycling at various current densities.

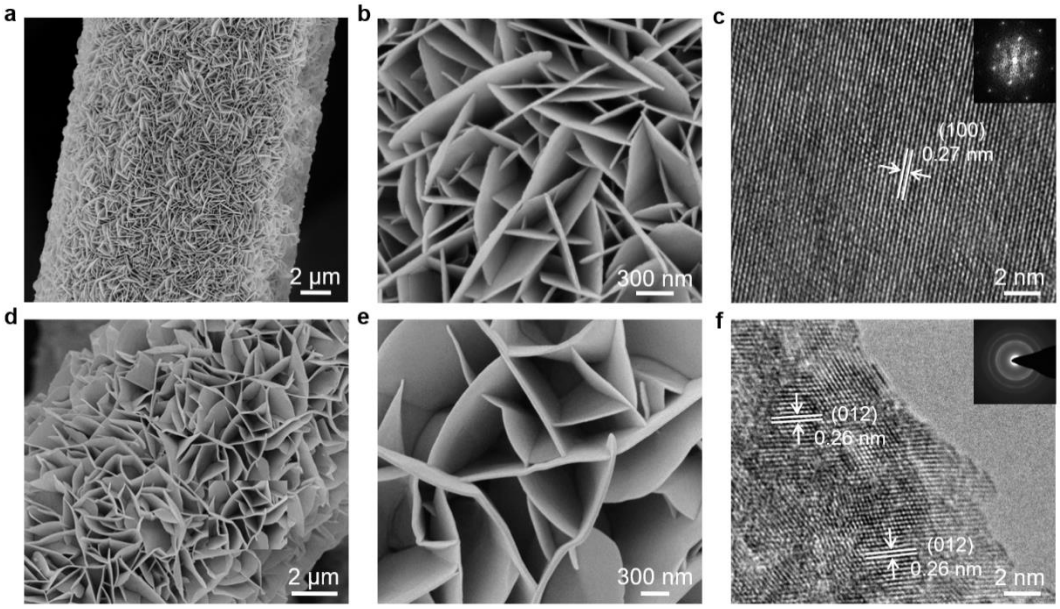

Figure S10. a, b) SEM and c) HR-TEM images of the regular β-$Ni(OH)_2$. d, e) SEM and f) HR-TEM images of the regular α-$Ni(OH)_2$. The inset is the FFT pattern taken from the corresponding HR-TEM region.

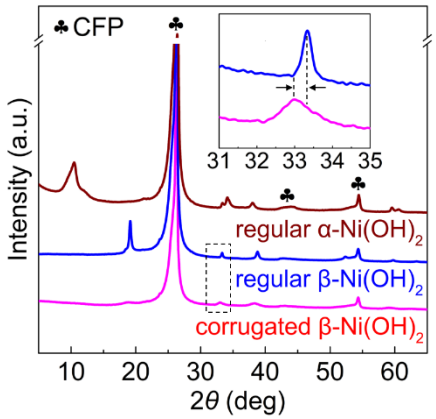

Figure S11. XRD patterns of regular α-$Ni(OH)_2$, β-$Ni(OH)_2$ and corrugated β-$Ni(OH)_2$.

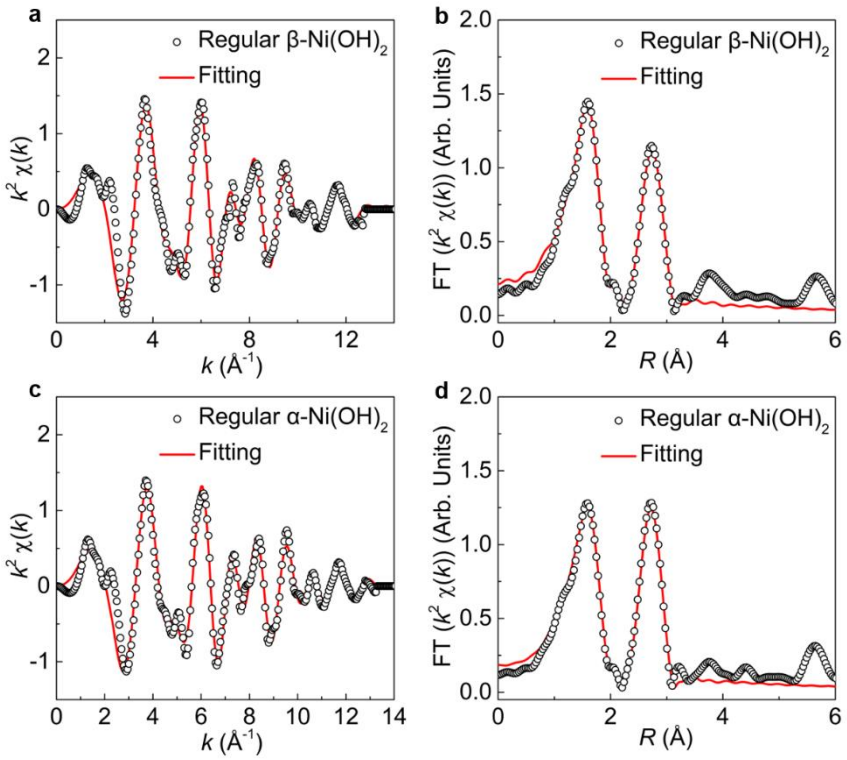

Figure S12. EXAFS $k^2\chi(k)$ oscillation curves and R space fitting results of Ni K-edge for regular a, b) β-$Ni(OH)_2$ and c, d) α-$Ni(OH)_2$ electrodes.

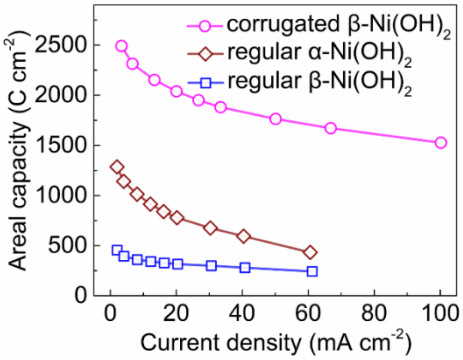

Figure S13. Areal capacity of the corrugated β-$Ni(OH)_2$, regular α-$Ni(OH)_2$ and β-$Ni(OH)_2$ at different current density.

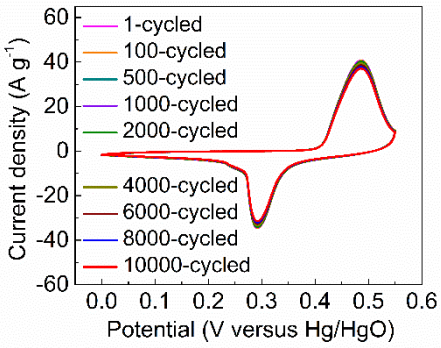

Figure S14. CV curves of the corrugated β-$Ni(OH)_2$ electrode after different cycles at scan rate of 5 mV s^{-1}.

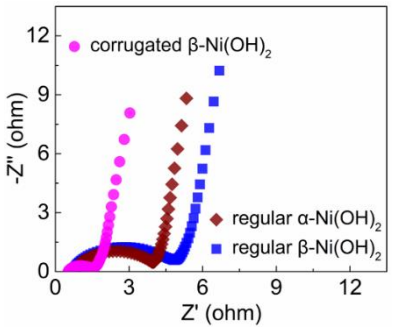

Figure S15. EIS spectra of regular α-$Ni(OH)_2$, β-$Ni(OH)_2$ and corrugated β-$Ni(OH)_2$.

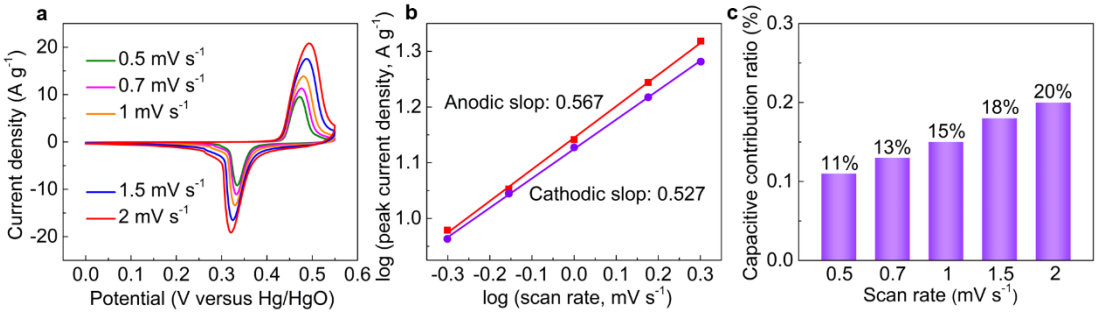

Figure S16. a) CV curves of the corrugated β-Ni(OH)$_2$ electrode at various scan rates of 0.5-2 mV s^{-1}. b) Logarithm of anodic and cathodic peak current densities versus logarithm of scan rates for the corrugated β-Ni(OH)$_2$ electrode. c) Capacitive contribution ratio to the cathodic peak current for the corrugated β-Ni(OH)$_2$ electrode.

The current response is described as a sum of two mechanisms (the capacitive and the diffusion-controlled processes) as described in the following equation:

$$i = k_1 v + k_2 v^{1/2} \quad (1)$$

where k_1 and k_2 are calculated values. The current is a combination of capacitive effects ($k_1 v$) and diffusion-controlled processes ($k_2 v^{1/2}$).

The equation (1) can be rearranged to equation as following:

$$i/v^{1/2} = k_1 v^{1/2} + k_2 \quad (2)$$

Thus, the value of k_1 and k_2 can be determined by plotting $v^{1/2}$ vs $i/v^{1/2}$. The ratio of the capacitive contribution to the peak current can be calculated by comparing the $k_1 v$ versus the peak current at different scan rates.

Table S1. EXAFS fitting results for the structural parameters around Ni atoms in NiV-LDH under different stages.

Sample	Path	*N*	*R*(Å)	σ^2 (10^{-3}Å)	ΔE_0 (eV)	*R*-factor
NiV-LDH	Ni-O	6.0±0.2	2.04±0.03	6.5±0.8	-5.2±0.8	0.006
	Ni-Ni/V	6.0±0.2	3.08±0.01	7.8±0.5	-1.8±0.9	
0.7-5	Ni-O	5.4±0.2	2.04±0.02	7.6±0.6	-4.9±0.8	0.012
	Ni-Ni/V	5.1±0.1	3.12±0.01	6.7±0.5	-1.0±0.9	
0.7-9	Ni-O	5.0±0.2	2.04±0.04	10.5±1.3	-3.0±0.8	0.015
	Ni-Ni/V	4.5±0.1	3.15±0.01	6.4±0.5	-1.1±0.8	

N is the coordination number; *R* is interatomic distance (the bond length between Co central atoms and surrounding coordination atoms; σ^2 is Debye-Waller factor (represents the thermal and static disorder in absorber-scatterer distances); ΔE_0 is edge-energy shift (the difference between the zero kinetic energy value of the sample and that of the theoretical model). *R* factor is used to assess the goodness of the fitting.

Table S2. EXAFS fitting results for the structural parameters around Ni atoms in regular β-$Ni(OH)_2$ and α-$Ni(OH)_2$.

Sample	Path	*N*	*R*(Å)	σ^2 (10^{-3}Å)	ΔE_0 (eV)	*R*-factor
β-$Ni(OH)_2$	Ni-O	6.0±0.2	2.04±0.05	5.5±0.8	-7.0±0.9	0.003
	Ni-Ni	6.0±0.2	3.10±0.02	8.6±0.5	-4.5±0.9	
α-$Ni(OH)_2$	Ni-O	6.0±0.2	2.04±0.04	6.8±0.8	-5.2±0.9	0.007
	Ni-Ni	6.0±0.2	3.09±0.01	7.8±0.5	-1.8±0.9	

Table S3. A comparison of electrochemical performance for the corrugated β-$Ni(OH)_2$ electrodes with some representive $Ni(OH)_2$-based electrodes in literature.

Sample	Voltage (V)	Electrolyte	Electrochemical performance			Sample
			Specific capacitance	Capacitance retention	Stability	
corrugated β-$Ni(OH)_2$ nanosheets	0.55 V vs. Hg/HgO	6 M KOH	746 C g^{-1} at 1 A g^{-1}	corrugated β-$Ni(OH)_2$ nanosheets	0.55 V vs. Hg/HgO	This work
β-$Ni(OH)_2$	0.4 V vs. Hg/HgO	3 M KOH	210 C g^{-1} at 1 A g^{-1}	β-$Ni(OH)_2$	0.4 V vs. Hg/HgO	[1]
β-$Ni(OH)_2$@PPy	0.50 V vs. Hg/HgO	3 M KOH	467 C g^{-1} at 1 A g^{-1}	β-$Ni(OH)_2$@PPy	0.50 V vs. Hg/HgO	[2]
β-$Ni(OH)_2$-graphene mixture	0.48 V vs. Ag/AgCl	1 M KOH	326 C g^{-1} at 1.4 A g^{-1}	β-$Ni(OH)_2$-graphene mixture	0.48 V vs. Ag/AgCl	[3]
α-$Ni(OH)_2$ nanosheets	0.45 V vs. Hg/HgO	6 M KOH	720 C g^{-1} at 2 mV s^{-1}	α-$Ni(OH)_2$ nanosheets	0.45 V vs. Hg/HgO	[4]
α-$Ni(OH)_2$/NF	0.4 V vs Hg/Hg_2Cl_2	6 M KOH	400 C g^{-1} at 2.5 A g^{-1}	α-$Ni(OH)_2$/NF	0.4 V vs Hg/Hg_2Cl_2	[5]
α-$Ni(OH)_2$ and β-$Ni(OH)_2$ mixture	0.47 V vs. SCE	1 M KOH	665 C g^{-1} at 1 A g^{-1}	α-$Ni(OH)_2$ and β-$Ni(OH)_2$ mixture	0.47 V vs. SCE	[6]
Co-doped α-$Ni(OH)_2$/CF	0.45 V vs. Hg/HgO	2 M KOH	495 C g^{-1} at 5 A g^{-1}	Co-doped α-$Ni(OH)_2$/CF	0.45 V vs. Hg/HgO	[7]
Co-doped α-$Ni(OH)_2$/rGO	0.45 V vs. Ag/AgCl	2 M KOH	515 C g^{-1} at 5 A g^{-1}	Co-doped α-$Ni(OH)_2$/rGO	0.45 V vs. Ag/AgCl	[8]
$NiCo_2O_4$ microtubes	0.53 V vs. SCE	2 M KOH	735 F g^{-1} at 2 A g^{-1}	$NiCo_2O_4$ microtubes	0.53 V vs. SCE	[9]
β-$Ni(OH)_2$ microspheres	0.5 V vs. Hg/HgO	6 M KOH	605 C g^{-1} at 1 A g^{-1}	β-$Ni(OH)_2$ microspheres	0.5 V vs. Hg/HgO	[10]
NiCoMn hydroxide nanosheets	0.5 V vs. Hg/HgO	6 M KOH	594 C g^{-1} at 1 A g^{-1}	NiCoMn hydroxide nanosheets	0.5 V vs. Hg/HgO	[11]
α-$Ni(OH)_2$	0.52 V vs. Hg/HgO	6 M KOH	565 C g^{-1} at 1 A g^{-1}	α-$Ni(OH)_2$	0.52 V vs. Hg/HgO	[12]
β-$Ni(OH)_2$-NF	0.4 V vs. SCE	6 M KOH	373 C g^{-1} at 4 A g^{-1}	β-$Ni(OH)_2$-NF	0.4 V vs. SCE	[13]
α-$Ni(OH)_2$/CF	0.45 V vs. Hg/HgO	1 M KOH	243 C g^{-1} at 1 A g^{-1}	α-$Ni(OH)_2$/CF	0.45 V vs. Hg/HgO	[14]
α-Co/$Ni(OH)_2$@Co_3O_4	0.6 V vs. Ag/AgCl	6 M KOH	500 C g^{-1} at 1 A g^{-1}	α-Co/$Ni(OH)_2$@Co_3O_4	0.6 V vs. Ag/AgCl	[15]

References

[1] Q. Liu, C. Chen, J. Zheng, L. Wang, Z. Yang, W. Yang, *J. Mater. Chem. A* **2017**, *5*, 1421.

[2] W. He, G. Zhao, P. Sun, P. Hou, L. Zhu, T. Wang, L. Li, X. Xu, T. Zhai, *Nano Energy* **2019**, *56*, 207.

[3] H. Wang, H. S. Casalongue, Y. Liang, H. Dai, *J. Am. Chem. Soc.* **2010**, *132*, 7472.

[4] J. Yan, Z. Fan, W. Sun, G. Ning, T. Wei, Q. Zhang, R. Zhang, L. Zhi, F. Wei, *Adv. Funct. Mater.* **2012**, *22*, 2632.

[5] K. Zhou, W. Zhou, L. Yang, J. Lu, S. Cheng, W. Mai, Z. Tang, L. Li, S. Chen, *Adv. Funct. Mater.* **2015**, *25*, 7530.

[6] N. A. Alhebshi, R. B. Rakhi, H. N. Alshareef, *J. Mater. Chem. A* **2013**, *1*, 14897.

[7] T. Li, W. Zhang, L. Zhi, H. Yu, L. Dang, F. Shi, H. Xu, F. Hu, Z. Liu, Z. Lei, J. Qiu, *Nano Energy* **2016**, *30*, 9.

[8] B. Zhao, L. Zhang, Q. Zhang, D. Chen, Y. Cheng, X. Deng, Y. Chen, R. Murphy, X. Xiong, B. Song, C.-P. Wong, M.-S. Wang, M. Liu, *Adv. Energy Mater.* **2018**, *8*, 1702247.

[9] F.-X. Ma, L. Yu, C.-Y. Xu, X. W. Lou, *Energy Environ. Sci.* **2016**, *9*, 862.

[10] Z. Xiao, Y. Mei, S. Yuan, H. Mei, B. Xu, Y. Bao, L. Fan, W. Kang, F. Dai, R. Wang, L. Wang, S. Hu, D. Sun, H.-C. Zhou, *ACS Nano* **2019**, *13*, 7024.

[11] P. Sivakumar, M. Jana, M. G. Jung, A. Gedanken, H. S. Park, *J. Mater. Chem. A* **2019**, *7*, 11362.

[12] Y. Zhu, C. Huang, C. Li, M. Fan, K. Shu, H. C. Chen, *J. Power Sources* **2019**, *412*, 559.

[13] Y. Ouyang, X. Yang, Y. Yi, Y. Zhang, W. Lei, Q. Hao, *J. Electrochem. Soc.* **2020**, *167*, 020560.

[14] Y. Zhou, S. Zhao, X. Yu, Y. Li, H. Chen, L. Han, *Inorg. Chem. Front.* **2020**, *7*, 427.

[15] Y. Bao, Y. Deng, M. Wang, Z. Xiao, M. Wang, Y. Fu, Z. Guo, Y. Yang, L. Wang, *Appl. Surf. Sci.* **2020**, *504*, 144395.